Tetrahedron xxx (xxxx) xxx

Contents lists available at ScienceDirect

Tetrahedron

journal homepage: www.elsevier.com/locate/tet

Stereoisomerization of human constitutive androstane receptor agonist CITCO

Benjamin Diethelm-Varela [a], Anmol Kumar [a], Caitlin Lynch [b], Gregory H. Imler [c], Jeffrey R. Deschamps [c], Yue Li [d], Menghang Xia [b], Alexander D. MacKerell Jr. [a], Fengtian Xue [a, *]

[a] Department of Pharmaceutical Sciences, University of Maryland School of Pharmacy, 20 Penn Street, Baltimore, MD, 21201, United States
[b] National Center for Advancing Translational Sciences, National Institutes of Health, Bethesda, MD, 20892-3375, United States
[c] Naval Research Laboratory, Code 6930, 4555 Overlook Avenue, Washington, D.C., 20375, United States
[d] Department of Chemistry and Biochemistry, University of Maryland College Park, College Park, MD, 20740, USA

ARTICLE INFO

Article history:
Received 30 October 2020
Accepted 11 December 2020
Available online xxx

ABSTRACT

CITCO (6-(4-chlorophenyl)imidazo[2,1-*b*][1,3]thiazole-5-carbaldehyde-O-(3,4-dichlorobenzyl) oxime) is a widely used agonist of the human constitutive androstane receptor (hCAR), a key hepatic xenobiotic sensor protein with emerging therapeutic indications. To address the insufficient stability of CITCO, which limits its therapeutic potential, the *E*- and *Z*-isomers of CITCO were synthesized and characterized by X-ray crystallography, one- and two-dimensional NMR spectroscopy. The two isomers were found to undergo *E/Z* isomerizations in solution likely via a protonation-rotation mechanism, time- and concentration-dependently. Our molecular modeling studies suggests both stereoisomers can bind to hCAR.

1. Introduction

CITCO (6-(4-chlorophenyl)imidazo[2,1-*b*][1,3]thiazole-5-carbaldehyde-O-(3,4-dichlorobenzyl) oxime) was first discovered by Maglich and coworkers in 2003 [1]. Since its introduction, it has been widely used as a selective agonist for the human constitutive androstane receptor (hCAR), a key hepatic xenobiotic sensor that plays important regulatory roles in drug metabolism and activation, glucose and lipid homeostasis, and cell fate [2–5]. Recently Lin and coworkers reported that CITCO also directly activates the human pregnane X receptor (hPXR), another important xenobiotic receptor [6]. As a small molecule tool, CITCO has been involved in numerous studies regarding biological regulation of hCAR by different proteins (e.g., PP2A, [7] ATF5, [8] DAX1, [9] MPR4[10], and EGFR [11]) and protein complexes (e.g., proteasome [12] and WNT/β-catenin [13]). It has also been used to elucidate the role of hCAR in regulating its target genes, [14–17] and other molecules such as P-glycoprotein, multidrug resistance protein, [18] and steroid hormones [19].

Upon xenobiotic activation, hCAR regulates the expression of various hepatic genes that encode important enzymes involved in phase I oxidation, phase II conjugation, and phase III drug transporters [20,21]. Therefore, selective modulation of hCAR has become a pharmacological strategy to enhance the metabolic efficiency of drugs [22]. This strategy was highlighted by the development of hCAR ligands as metabolic enhancers of the chemotherapy cyclophosphamide [23]. As a positive control, CITCO was implicated in the development of various biological assays of hCAR [24–28] and in the discovery of hCAR ligands including agonists, [29–35] antagonists, [36,37] and inverse agonists [36,38]. Recently using the chemical scaffold of CITCO as a parent, efforts have emerged in the development of novel potent and selective agonists of hCAR [39,40].

The binding of CITCO to the ligand binding domain (LBD) of hCAR was confirmed by direct-binding assays including fluorescence resonance energy transfer (FRET) and surface plasmon resonance (SPR) [1]. The crystal structure of CITCO in complex with the LBD of hCAR has also been solved [41]. The chemical structure of CITCO contains an oxime functionality connecting the imidazo [2,1-*b*]thiazole and dichlorobenzyl moieties (Fig. 1). Interestingly, while both *E*- and *Z*-isomers around the oxime double bond are possible, in the literature CITCO has been displayed exclusively as

* Corresponding author.
E-mail address: fxue@rx.umaryland.edu (F. Xue).

https://doi.org/10.1016/j.tet.2020.131886
0040-4020/

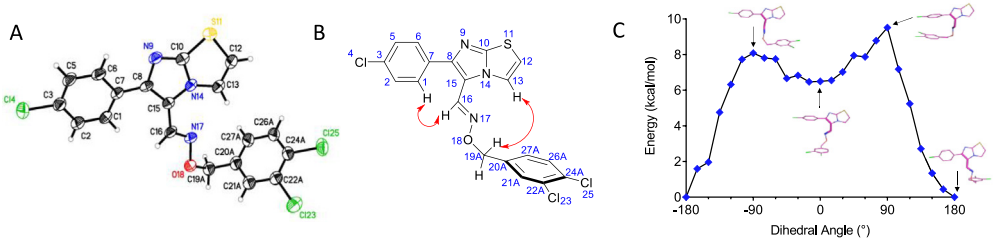

Fig. 1. A. Single crystal structure of *E*-CITCO. B. Schematized through-space interactions detected using NOESY spectroscopy. NOESY crosspeaks that link protons are represented as red arrows. C. Potential energy scan of the dihedral "C8–C15–C16–N17" in the range of −180° degree to 180° degree at HF/6-31G(d) model chemistry using Psi4 package [43]. This potential energy scan spans through conversion of *cis*-to *trans*-conformation of *E*-CITCO, where dihedral value of 180° (or −180°) implies *trans*-rotamer of two chlorinated moieties and 0° implies *cis*-rotamer. Four different conformations with "C8–C15–C16–N17" dihedral values −90°, 0°, 90° and 180° are projected on the plot.

the *E*-isomer, although no experimental evidence was documented [1,23,41].

2. Results and discussion

We synthesized CITCO via a condensation reaction of 6-(4-chlorophenyl)imidazo[2,1-*b*]thiazole-3-carbaldehyde and O-(3,4-dichlorobenzyl)hydroxylamine in the presence of AcOH at 70 °C (Scheme S1, Table 1) [39,42]. The ^{1}H-NMR data indicated the formation of a single product with signals compatible to that of CITCO (Fig. S1). This product was successfully crystallized and confirmed by X-ray diffraction studies as *E*-CITCO, with a *trans*-configuration at the oxime double bond C_{16}═N_{17} (Fig. 1A). The molecule adopts an overall τ-shaped geometry, with the hydrogen atoms on C_1 (H_1) and C_{16} (H_{16}) close to each other, and the dichlorobenzyl moiety pointing toward the imidazothiozole core. It is worth noting that the configuration of *E*-CITCO in the single crystal was significantly different to the one reported in the cocrystal structure of *E*-CITCO in hCAR, in which the dichlorobenzyl group was in close proximity to the *p*-chlorophenyl ring [41]. The crystallographic result was supported by NOESY spectroscopy in either aqueous environment (10% D_2O in DMSO, Fig. 1B and S19) or organic solvent ($CDCl_3$) (Fig. S21), which indicated through-space interactions between hydrogen pairs H_1/H_{16} and H_{13}/H_{19A}, while no interactions were detected between the imidazothiazole and dichlorophenyl rings. It was interesting that the same *trans* rotamer, in which a through-space interaction observed between H_1 and H_{16}, was present in both solid and solution environments. These experimental observations were further confirmed by our quantum mechanics (QM) simulation studies. As shown in Fig. 1C, the calculated energy for the *trans*-rotamer was −6.5 kcal/mol lower than that of the *cis*-rotamer.

Next we sought to screen conditions for the synthesis of CITCO (Table 1). Removal of AcOH from the reaction condition caused a significant decrease of yields, while a reaction performed at room temperature only indicated a slight decrease of yields. Changing the solvent from EtOH to MeOH showed no obvious impact on reaction yields, however reactions employing other solvents such as dioxane and toluene showed decreased yields. Interestingly, we found that under all tested conditions, CITCO was generated exclusively as the *E*-isomer, and this stereoselectivity remained during the formation of other oximes and the corresponding imine analog (Table S1). Therefore, the condensation reaction for the formation of CITCO probably has a kinetic drive that favors the formation of *E*-CITCO.

Table 1
Conditions for the synthesis of CITCO.

solvent	Additives	temp (°C)	yield[a] (%)	*E* or *Z*[b]
EtOH	AcOH	70	40	*E*
EtOH	–	70	26	*E*
EtOH	AcOH	rt	35	*E*
MeOH	AcOH	70	35	*E*
dioxane	AcOH	70	22	*E*
toluene	AcOH	70	29	*E*

[a] The low yield was due to a common deformylation reaction of the starting material aldehyde, yielding *p*-chlorophenyl imidazothiazole as a byproduct (Scheme S2, and Figs. S2 and S3).
[b] Stereoselectivity determined by analysis of the ^{1}H-NMR spectra.

In the ^{1}H NMR spectrum of *E*-CITCO in $CDCl_3$, measured one day after dissolution, two sets of signals with different relative intensities were observed. A time-course of the NMR spectra showed the original set of signals decreased over time while the newly formed signal set increased (Fig. S4A). Conversely, the high-resolution mass spectra of the same NMR sample showed the presence of the peak at *m/z* 435.9477, corresponding to CITCO, while no other peaks were observed (Fig. S4B). The new compound was purified and successfully crystallized. The X-ray single crystallographic result revealed that the new compound was *Z*-CITCO, with the oxime double bond C_{16}═N_{17} adopting a *cis*-configuration (Fig. 2A). While the overall structure of *Z*-CITCO employed a similar configuration to that of *E*-CITCO, the distance between the imidazo[2,1-*b*]thiazole and dichlorobenzyl groups was shorter in *Z*-CITCO compared to that in the *E*-isomer. This result was also confirmed by NOESY experiments (Fig. 2B, S20, and S21), in which new through-space interactions between hydrogen pairs H_{12}/H_{21} and H_{13}/H_{27} were observed in addition to those detected in *E*-CITCO.

In an attempt to elucidate the agonistic activity of both CITCO stereoisomers for hCAR, we performed luciferase reporter-based activation assays using purified *E*- and *Z*-isomers along with the commercially available CITCO (*E*-isomer). No obvious difference was detected among the three samples, with the EC_{50} and E_{max} values falling within the same order of magnitude (Fig. 3). While this result might suggest both stereoisomers are equipotent, the aforementioned stereoisomerization could also play an important role. To better understand this reaction, a study of the isomerization kinetics was undertaken using ^{1}H-NMR spectroscopy.

The kinetic and mechanistic studies of oxime isomerizations are known [44–47]. Two distinct mechanisms, nucleophilic catalysis and protonation-rotation, are proposed for the isomerization reactions (Scheme S3). As shown in Fig. 4, at the concentration of 16 mM in $CDCl_3$, continuous isomerization reactions proceeded until equilibriums were reached with an approximate 20/80 (*E*/*Z*) ratio of the two isomers. The reaction half-lives $t_{1/2}$ were 17 and 8.1 days for *E*- and *Z*-CITCO, respectively (Table 2). The Gibbs free energy $\Delta G_{Z\text{-}E}$, as determined from the corresponding equilibrium constant *K*, were 3.4 and 3.8 kJ/mol, indicating the *Z*-isomer was favored under this condition.

Changing the solvent to DMSO-d_6 caused no significant difference in the kinetics of isomerization (Table 2 and Fig. S5). The addition of D_2O as a co-solvent indicated no detectable effect in

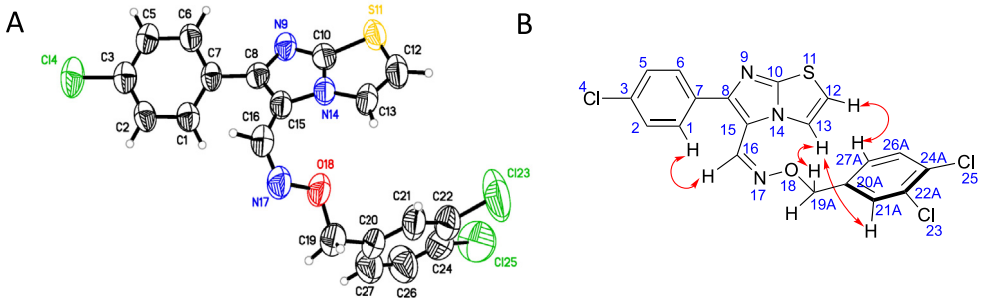

Fig. 2. A. Single crystal structure of *Z*-CITCO. B. Schematized through-space interactions detected using NOESY spectroscopy. NOESY cross peaks that link protons are represented as red arrows.

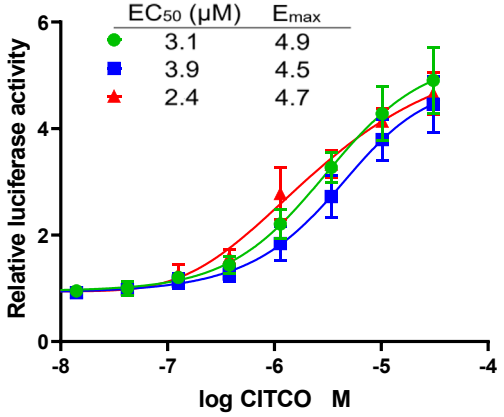

Fig. 3. Dose-dependent activation of hCAR by CITCO samples in an hCAR agonist luciferase gene reporter assay. Green: commercial CITCO; blue; *Z*-CITCO: red: *E*-CITCO. The incomplete dose response curves were due to the limited solubility of the samples.

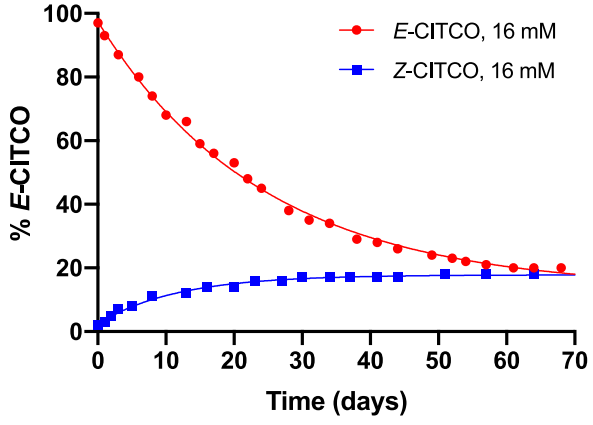

Fig. 4. Isomerization kinetics of CITCO (16 mM) in $CDCl_3$ at room temperature. The ^{1}H-NMR spectra were recorded over time at room temperature. The proportion of each isomer was estimated by NMR.

isomerization kinetics, suggesting that the isomerization rate is probably not dependent on nucleophilic catalysis. While inclusion of the base triethylamine (Et_3N) showed no impact on $t_{1/2}$, the isomerization reached a new equilibrium containing more *E*-isomer with the *K* and $\Delta G_{Z\text{-}E}$ values of 0.33 and 2.7 kJ/mol, respectively. Interestingly, the addition of trifluoroacetic acid (TFA) to the

Table 2
Kinetics of the isomerization of *E*-CITCO (16 mM) in $CDCl_3$[a].

additive	$t_{1/2}$ (days)	k (day^{-1})	K ([E]/[Z])	$\Delta G_{Z\text{-}E}$ (KJ/mol)
–	17	0.041	0.25	3.4
-[b]	8.1	0.086	0.21	3.8
DMSO-d_6[c]	16	0.044	0.23	3.7
D_2O, 2%	20	0.036	0.25	3.4
D_2O, 4%	19	0.038	0.26	3.4
Et_3N	17	0.042	0.33	2.7
TFA	6.2	0.11	1.9	−1.6

[a] All experiments were conducted at room temperature.
[b] *Z*-CITCO was used.
[c] The experiment was performed in DMSO-d_6.

reaction dramatically changed kinetics of the isomerization reaction. In the presence of 1 equiv of TFA, the reaction proceeded much faster with the $t_{1/2}$ value of 6.2 days, indicating that the isomerization likely went through an acid-catalyzed protonation-rotation mechanism. Meanwhile at equilibrium, the *E*-CITCO predominated the mixture with the *K* and $\Delta G_{Z\text{-}E}$ values of 1.9 and −1.6 kJ/mol, respectively.

Next, a concentration-dependency study was performed (Fig. 5 and Table 3). The $t_{1/2}$ values of the isomerization reaction were significantly dependent on the concentration, ranging between 0.1 and over 50 days. For reactions beginning with a concentration of 2.5 mM or higher, at equilibrium the *Z*-isomer predominated ($K < 0.5$). The fraction of *E*-isomer increases when the concentration decreases. Meanwhile, shorter reaction times were required to reach equilibrium when starting with less concentrated samples (see Fig. S6 for full time courses). The concentration dependency was pronounced; the sample with a concentration of 2.5 mM showed $t_{1/2} = 1.1$ days compared to $t_{1/2} = 17$ days of 16 mM, which accounts for an over 6-fold increase in time necessary to reach half the equilibrium concentration. When the concentration was near the solubility of CITCO (110 mM) in $CDCl_3$, no obvious isomerization was evidenced by NMR spectroscopy over a 40-day period (data not shown). Conversely, at the concentration of 100 μM in either $CDCl_3$ or aqueous DMSO-d_6 that broadly mimics conditions used for biological tests, rapid isomerizations were observed with equilibriums being reached in 0.1 and 0.3 days, respectively. These results can explain the apparently identical agonistic activity of both *E*- and *Z*-isomers determined by the luciferase reporter assays, which involve low to medium micromolar concentrations of the testing compounds, and require an incubation period of 24 h [48].

These experiments also revealed that the equilibrium position is concentration-dependent. At higher concentrations, the *Z*-isomer seems to be favored in solution, as the equilibrium leads to over 80% of this isomer. At lower concentrations, such as 2.5 mM and 100 μM, the percentage of *Z*-isomer in the mixture decreased to

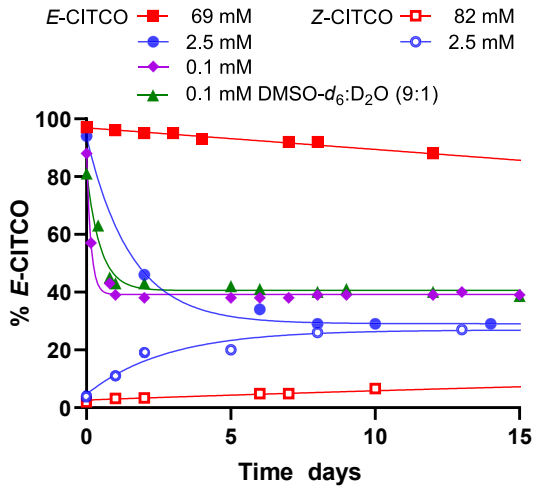

Fig. 5. Isomerization kinetics of *E*- and *Z*-CITCO at different concentrations.

Table 3
Kinetics studies of *E*- or *Z*-CITCO at different concentrations in $CDCl_3$[a].

conc. (mM)	$t_{1/2}$ (days)	k (day^{-1})	K ([E]/[Z])	$\Delta G_{Z\text{-}E}$ (KJ/mol)
69 (*E*)[b]	>50	–	–	–
2.5 (*E*)	1.1	0.65	0.41	2.2
0.1 (*E*)	0.11	6.6	0.63	1.2
0.1 (*E*)[c]	0.33	2.1	0.71	0.83
82 (*Z*)[b]	>50	–	–	–
2.5 (*Z*)	1.9	0.36	0.37	2.5

[a] All experiments were conducted at room temperature.
[b] Experiments were stopped at day 50 and data points were not enough to produce accurate fits.
[c] The NMR sample was dissolved in 10% D_2O in DMSO-d_6.

approximately 70% and 60%, respectively. Thus, an interplay between the thermodynamic (equilibrium position) and kinetic (isomerization rate) parameters is evident in this process, where the higher the concentration, the more favored the *Z*-isomer is.

Taken together our X-ray crystallographic and NMR results provide direct experimental evidence for the formation and isomerization of CITCO (Scheme 1). CITCO is generated, via a condensation reaction of 6-(4-chlorophenyl)imidazo[2,1-*b*]thiazole-3-carbaldehyde and O-(3,4-dichlorobenzyl)hydroxylamine, as the *E*-isomer, which was a kinetic product with the least steric strain. After formation, both *E*- and *Z*-CITCO can undergo a time- and concentration-dependent isomerization in solution, likely following a protonation-rotation mechanism.

The results from the kinetic studies prompted us to revisit the binding mode of CITCO by docking both isomers into the reported electron density map (Fig. 6) [41]. Compared to the binding mode of *E*-CITCO proposed in the original cocrystal structure (Fig. 6A), our docking studies predicted *E*-CITCO to adopt a highly similar binding mode (Fig. 6B), with the dichlorobenzyl and *p*-chlorophenyl groups close to each other. Interestingly, the *Z*-isomer was also predicted to bind favorably to the LBD of hCAR, although with a different inversed binding mode (Fig. 6C), in which the *p*-chlorophenyl and imidazo[2,1-*b*]thiazole groups bound in opposite positions to those shown in *E*-CITCO.

In summary, we have shown that the widely-used hCAR activator CITCO was synthesized exclusively as the *E*-stereoisomer. Both *E*- and *Z*-isomers undergo time- and concentration-dependent stereoisomerization through a protonation-rotation mechanism, leading to an equilibrium position. Given the rapid rate of isomerization at low concentration, it must be noted that every biological measurement done with CITCO thus far likely stems from a mixture of isomers, with the activity of each still being unknown. Our computational simulations suggest the existence of unique binding poses for each isomer, both of which match the experimental electron-density of the published crystal structure. In order to properly understand the biological properties of this compound, and to arrive at a three-dimensional pharmacophore, future studies will involve the synthesis of stable CITCO-like stereoisomers.

3. Experimental section

3.1. General procedures

All reagents and solvents were of analytical grade and used without further purification. Reactions were monitored using thin-layer chromatography (TLC) on commercial silica-gel plates (GF254). Flash column chromatography was performed on silica gel (200–300 mesh). NMR spectra were obtained on a Varian INOVA 400 MHz NMR spectrometer at 25 °C. Chemical shifts are reported as δ values (parts per million) using the residual solvent peak as an internal reference. Chemical shifts (δ) were reported in ppm referenced to the $CDCl_3$ residual peak (δ 7.264) for ^1H NMR. Chemical shifts of ^{13}C NMR were reported relative to $CDCl_3$ (δ 77.04). Data for ^1H NMR were reported in the following order: chemical shift, multiplicity (s, singlet; d, doublet; t, triplet; sext, sextet; m, multiplet), coupling constant (Hz), number of protons. Data for ^{13}C NMR were reported as δ values (parts per million). High-resolution mass spectra (HRMS) were obtained on a JEOL AccuTOF with ESI/APCI ion sources coupled to an Agilent 1100 HPLC system. HPLC analysis was performed on a Shimadzu HPLC fitted

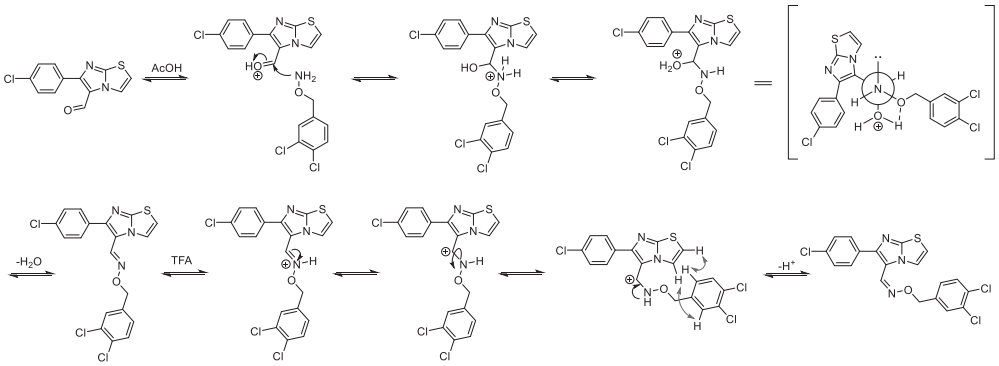

Scheme 1. Proposed Mechanism for *E*-CITCO Formation and Stereoisomerization.

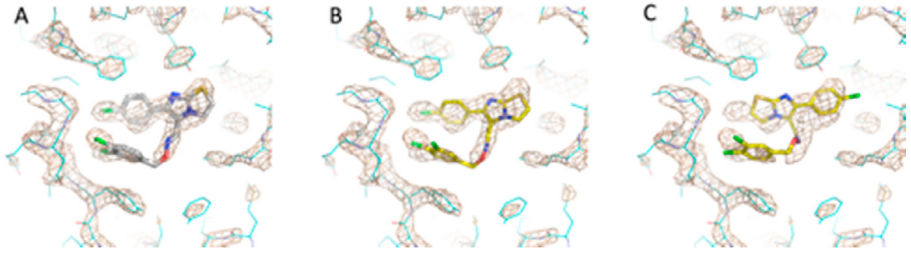

Fig. 6. Comparison of published binding mode of CITCO (A) to docking results of *E*-CITCO (B) and Z-CITCO (C) using the software AutoDock Vina, overlaid on the electron-density map of hCAR (yellow mesh).

with a C-18 reversed-phase column (Phenomenex, luna 5 μM C18(2) 4.6 mm × 100 mm) with a flow rate of 0.8 mL/min using CH_3CN—H_2O 8:2 mobile phase. The purity of final products is >95%.

3.2. Synthesis

3.2.1. 6-(4-Chlorophenyl)imidazo[2,1-b]thiazole

This compound was synthesized by following a procedure that has been reported [39]. To a solution of 4-chloro-2-bromoacetophenone (15 mmol) in EtOH (15 mL) was added 2-aminothiazole (15 mmol). The reaction mixture was heated under reflux for 24 h and cooled down. The solvent was removed under vacuum, and the resulting material was partitioned between saturated $NaHCO_3$ (20 mL) and EtOAc (20 mL). The aqueous layer was extracted by EtOAc (2 × 20 mL) and the combined organic layers were dried over anhydrous Na_2SO_4, and concentrated. The crude product was purified by flash chromatography using EtOAc/hexanes (1:4) to yield the titled product as a yellow solid. Yield: 2.8 g (80%).

3.2.2. 6-(4-Chlorophenyl)imidazo[2,1-b]oxazole

This compound was synthesized by following a procedure that has been reported [39]. A solution of oxazol-2-amine (5 mmol) and bromomethyl ketone (5 mmol) in THF (20 mL) and CH_3CN (30 mL) was stirred at room temperature for 24 h. The precipitate from the reaction mixture was collected by filtration and the filtrate was washed using CH_3CN. To a solution of the resulting solid in toluene (50 mL) at 0 °C was added titanium (IV) chloride (5 mmol) as a solution in toluene (5 mL) dropwise over a period of 30 min. The reaction mixture was heated at 100 °C for an additional 3 h, and cooled. The solvent was removed by rotary evaporation, and ice was added to the residue. The pH value of the resulting mixture was adjusted to 9 using Na_2CO_3, and the resulting solution was extracted using EtOAc (30 mL × 3). The organic layers were combined and dried over anhydrous Na_2SO_4. The concentrated crude product was dried overnight under vacuum to get the crude product, which was purified by flash chromatography using EtOAc/hexanes (1:4) to yield the desired product as a white solid. Yield: 612 mg (56%).

3.2.3. O-(3,4-Dichlorobenzyl)hydroxylamine

This compound was synthesized by following a procedure that has been reported [49]. To a solution of sodium ethoxide (43 mmol) in EtOH (70 mL) was added *N*-hydroxyurethane (43 mmol) dropwise, followed by 3,4-dichlorobenzyl chloride (43 mmol). The reaction mixture was allowed to stir at room temperature for 10 h. A solution of sodium hydroxide (86 mmol) in water (70 mL) was added and the resulting suspension was heated under reflux for an additional 2 h. The EtOH was removed under vacuum and the resulting aqueous mixture was extracted by diethyl ether (3 × 100 mL). The combined organic layers were dried over anhydrous Na_2SO_4 and concentrated to 100 mL under vacuum. To the resulting solution, HCl in EtOH (5 mol/L, 8.5 mL) was added dropwise. The precipitate was filtered under and the filtrate was washed with diethyl ether to provide the desired product as white crystals. Yield: 6.2 g (75%).

3.2.4. 6-(4-Chlorophenyl)imidazo[2,1-b]thiazole-3-carbaldehyde

This compound was synthesized by following a procedure that has been reported [39]. To dimethyl formamide (179 mmol) in an ice-bath was added phosphorus (V) oxychloride (29.8 mmol) dropwise. The mixture was stirred for 5 min before the addition of 6-(4-chlorophenyl)imidazo[2,1-*b*]thiazole (12.4 mmol) as a solution in dimethyl formamide. The reaction mixture was warmed to room temperature, and vigorously stirred for 3 h, then potassium hydroxide (120 mmol) was added as a solution in water (3.8 M). The mixture was heated under reflux overnight, cooled, and poured over an ice bath. The resulting precipitate was collected by filtration under vacuum and washed generously with water to give the desired product as a white solid that was used in the next step without further purification. Yield: 3.1 g (95%).

3.2.5. 6-(4-Chlorophenyl)imidazo[2,1-b]oxazole-3-carbaldehyde

This compound was synthesized by following a procedure that has been reported [39]. To dimethyl formamide (15 mmol) in an ice-bath was added phosphorus (V) oxychloride (2.5 mmol) dropwise. The mixture was stirred for 5 min before the addition of 6-(4-chlorophenyl)imidazo[2,1-*b*]thiazole (1 mmol) as a solution in dimethyl formamide. The reaction mixture was warmed to room temperature, and vigorously stirred for 3 h, then potassium hydroxide (10 mmol) was added as a solution in water (3.8 M). The mixture was heated under reflux overnight, cooled, and poured over an ice bath. The resulting precipitate was collected by filtration under vacuum and washed generously by water to give the desired product as a white solid that was used in the next step without further purification. Yield: 234 mg (95%).

3.2.6. General procedure A: synthesis of Aryl-3-carbaldehyde O-Oximes

Procedure adapted from Liang and coworkers [39]. 6-(4-Chlorophenyl)imidazo[2,1-*b*]thiazole-3-carbaldehyde or (0.38 mmol) was dissolved in ethanol (5 mL). The corresponding hydroxylamine or amine (0.38 mmol) was added, followed by acetic acid (1.9 mmol). The mixture was heated at 70 °C for 16 h. The crude was partitioned between saturated $NaHCO_3$ and EtOAc and extracted with EtOAc three times. The combined organic layers were washed with brine and dried over anhydrous Na_2SO_4. The crude product was filtered and concentrated under vacuum. The resulting solid was purified by flash chromatography using 20% ethyl acetate in hexanes as the solvent system to yield the desired product as a white solid.

3.2.7. (E)-6-(4-Chlorophenyl)imidazo[2,1-b]thiazole-3-carbaldehyde O-(3,4-dichlorobenzyl) oxime (E-CITCO)

Synthesized through general procedure A using 6-(4-chlorophenyl)imidazo[2,1-*b*]thiazole-3-carbaldehyde and O-(3,4-dichlorobenzyl)hydroxylamine. ^{1}H NMR (400 MHz, $CDCl_3$): δ 8.39 (s, 1H), 7.99 (d, J = 4.5 Hz, 1H), 7.59 (d, J = 8.3 Hz, 2H), 7.51 (s, 1H), 7.46–7.42 (m, 3H), 7.24 (d, J = 6.3 Hz, 1H), 6.92 (d, J = 4.2 Hz, 1H), 5.14 (s, 2H); ^{13}C NMR (100 MHz, $CDCl_3$): δ 152.7, 149.3, 139.9, 137.7, 134.5, 132.6, 132.1, 131.9, 130.5, 130.1, 129.5, 129.0, 127.4, 121.6, 115.7, 113.0, 75.0. HRMS (ESI): Exact mass calcd for $C_{19}H_{12}Cl_3N_3OS$ [M + H$^+$] 434.9767, found 434.9477. Yield: 66 mg (40%).

As part of our synthetic study on the stereoselectivity in the synthesis of CITCO, the general procedure conditions were modified by substituting the solvent for either methanol, dioxane, or toluene, by omitting the acid additive, and by assaying the procedure at room temperature. The results in terms of yield and stereoselectivity are summarized on Table 1.

3.2.8. (Z)-6-(4-Chlorophenyl)imidazo[2,1-b]thiazole-3-carbaldehyde O-(3,4-dichlorobenzyl) oxime (Z-CITCO)

Synthesized through general procedure A using 6-(4-chlorophenyl)imidazo[2,1-b]thiazole-3-carbaldehyde and O-(3,4-dichlorobenzyl)hydroxylamine. The pure *E* stereoisomer was dissolved in acetone to a final concentration of 2.5 mM and left to isomerize for several days. *Z* stereoisomer was resolved by flash chromatography (36 mg). ^{1}H NMR (400 MHz, $CDCl_3$): δ 7.66 (d, J = 4.1 Hz, 1H), 7.59 (d, J = 8.3 Hz, 2H), 7.49–7.40 (m, 5H), 7.21 (d, J = 8.3 Hz, 1H), 6.81 (d, J = 4.5 Hz, 1H), 5.20 (s, 2H); ^{13}C NMR (100 MHz, $CDCl_3$): δ 152.5, 149.9, 137.1, 136.3, 134.6, 132.7, 132.4, 131.9, 130.6, 130.3, 129.9, 128.8, 127.6, 123.1, 115.0, 111.8, 75.3. HRMS (ESI): Exact mass calcd for $C_{19}H_{12}Cl_3N_3OS$ [M + H$^+$] 434.9767, found 434.9477.

3.2.9. 6-(4-Chlorophenyl)imidazo[2,1-b]thiazol-5-yl)-N-(3,4-dichlorophenethyl)methanimine

Synthesized through a procedure adapted from Liang and co-workers [39]. 6-(4-Chlorophenyl)imidazo[2,1-b]thiazole-3-carbaldehyde (0.38 mmol) was dissolved in ethanol. 2-(3,4-dichlorophenyl)ethanamine (0.38 mmol) was added, followed by acetic acid (1.9 mmol). The mixture was heated at 70 °C for 16 h. The crude was partitioned between saturated $NaHCO_3$ and EtOAc and extracted with EtOAc three times. The combined organic layers were washed with brine and dried over anhydrous Na_2SO_4. The crude product was filtered and concentrated under vacuum. The resulting solid was purified by flash chromatography using 20% ethyl acetate in hexanes as the solvent system to yield the desired product as a white solid. Yield: 119 mg (72%).

3.2.10. 6-(4-Chlorophenyl)imidazo[2,1-b]thiazole-5-carbaldehyde oxime

Synthesized through general procedure A using 6-(4-chlorophenyl)imidazo[2,1-*b*]thiazole-3-carbaldehyde and hydroxylamine hydrochloride. ^{1}H NMR (400 MHz, DMSO-d_6): δ 11.43 (s, 1H), 8.36 (s, 1H), 8.08 (d, J = 4.6 Hz, 1H), 7.71 (d, J = 7.9 Hz, 2H), 7.53 (d, J = 8.3 Hz, 2H), 7.46 (d, J = 4.2 Hz, 1H); ^{13}C NMR (100 MHz, DMSO-d_6): δ 151.4, 146.0, 138.6, 132.7, 132.4, 129.6, 128.8, 126.4, 121.0, 115.0. HRMS (ESI): Exact mass calcd for $C_{12}H_8ClN_3OS$ [M + H$^+$] 277.0077, found 277.0154. Yield: 60 mg (57%).

3.2.11. 6-(4-Chlorophenyl)imidazo[2,1-b]thiazole-5-carbaldehyde O-propyl oxime

Synthesized through general procedure A using 6-(4-chlorophenyl)imidazo[2,1-*b*]thiazole-3-carbaldehyde and *O*-propylhydroxylamine. ^{1}H NMR (400 MHz, $CDCl_3$): δ 8.35 (s, 1H), 8.16 (d, J = 4.0 Hz, 1H), 7.61 (d, J = 8.4 Hz, 2H), 7.42 (d, J = 8.4 Hz, 2H), 6.92 (d, J = 4.2 Hz, 1H), 4.14 (t, J = 6.7 Hz, 2H), 1.76 (sext, J = 7.0 Hz, 2H), 1.00 (t, J = 7.4 Hz, 3H). ^{13}C NMR (100 MHz, DMSO-d6): δ .152.3, 148.4, 138.5, 134.2, 132.1, 129.5, 128.9, 121.8, 116.3, 112.7, 76.2, 22.4, 10.4. Exact mass calcd for $C_{15}H_{14}ClN_3OS$ [M + H$^+$] 319.0546, found 319.0620. Yield: 60 mg (57%). Yield: 69 mg (57%).

3.2.12. 6-(4-Chlorophenyl)imidazo[2,1-b]oxazole-3-carbaldehyde O-(3,4-dichlorobenzyl) oxime

Synthesized through a procedure adapted from Liang and co-workers [39]. 6-(4-Chlorophenyl)imidazo[2,1-*b*]oxazole-3-carbaldehyde (0.38 mmol) was dissolved in ethanol. O-(3,4-dichlorobenzyl)hydroxylamine (0.38 mmol) was added, followed by acetic acid (1.9 mmol). The mixture was heated at 70 °C for 16 h. The crude was parti-tioned between saturated $NaHCO_3$ and EtOAc and extract-ed with EtOAc three times. The combined organic layers were washed with brine and dried over anhydrous Na_2SO_4. The crude product was filtered and concentrated under vacuum. The resulting solid was purified by flash chromatography using 20% ethyl acetate in hexanes to yield the desired product as a white solid. Yield: 42 mg (26%).

3.3. Isomerization time-course

Pure *E*- or *Z*-CITCO was weighted on an analytical scale and dissolved on an appropriate solvent. Catalysts were added as required, and additional solvent was added to achieve the desired concentration. Solution was transferred to an NMR tube, and an ^{1}H-NMR spectrum was immediately acquired employing a d1 = 5s and 16 total scans. The proportion of each stereoisomer was estimated by normalizing the methylene protons signal integral of the *E* isomer (^{1}H NMR (400 MHz, $CDCl_3$): δ 5.14 (s, 2H)) to a value of 1, and calculating the ratio of the relative integral of the methylene protons in the *Z* isomer (^{1}H NMR (400 MHz, $CDCl_3$): δ 5.20 (s, 2H)) to this value. Samples were kept at room temperature, and spectra were re-acquired at regular intervals. The proportion of each isomer was calculated with each acquisition as described.

3.4. X-ray crystallography

Single-crystal X-ray diffraction data on compounds were collected using Cu Kα radiation and a Bruker Photon II CPAD area detector. The crystals were prepared for data collection by coating with high viscosity microscope oil. The oil-coated crystals were mounted on a micro-mesh mount (MiteGen, Inc.) and transferred to the diffractometer and a data set collected at 150 K for *E*-CITCO and 293 K for *Z*-CITCO. The structures were solved by direct methods and refined by full-matrix least squares on F [2] values using the programs found in the SHELXL suite (Bruker, SHELXL v2014.7, 2014, Bruker AXS Inc., Madison, WI). Corrections were applied for Lorentz, polarization, and absorption effects. Parameters refined included atomic coordinates and anisotropic thermal parameters for all non-hydrogen atoms. The H atoms were included using a riding model. Complete information on data collection and refinement is available in the supplemental material.

3.4.1. E-CITCO

The 0.070 × 0.027 × 0.010 mm^3 crystal was monoclinic in space group C2/c, with unit cell dimensions a = 35.774(11) Å, b = 6.935(3) Å, c = 20.419(4) Å, α = 90°, β = 121.277(14)°, and γ = 90°. Data was 95.5% complete to 67.679° θ with an average redundancy of 2.91. The final anisotropic full matrix least-squares refinement on F [2] with 372 variables converged at R_1 = 7.27%, for the observed data and wR2 = 19.38% for all data.

3.4.2. Z-CITCO

The 0.078 × 0.021 × 0.020 mm^3 crystal was monoclinic in space group $P2_1/c$, with unit cell dimensions a = 17.0194(12) Å, b = 7.1790(5) Å, c = 32.056(2) Å, $\alpha = 90^\circ$, $\beta = 100.064(4)^\circ$, and $\gamma = 90^\circ$. Data was 80.1% complete to 67.679° θ with an average redundancy of 2.31. The final anisotropic full matrix least-squares refinement on F [2] with 536 variables converged at $R_1 = 9.34\%$, for the observed data and wR2 = 32.91% for all data.

3.5. hCAR agonist luciferase reporter gene assay

HepG2-CYP2B6-hCAR [48] cells were cultured in DMEM (Invitrogen, Carlsbad, CA) supplemented with 5 μg/mL blasticidin (Invitrogen), 0.5 mg/mL geneticin (Invitrogen), 10% Hyclone™ FBS (GE Healthcare Life Sciences, Logan, UT), and 100 U/mL penicillin and 100 μg/mL streptomycin (Invitrogen). For the assay, the HepG2-CYP2B6-hCAR cells were dispensed at 2500 cells/4 μL/well in tissue culture−treated 1536-well white assay plates (Greiner Bio-One North America, Monroe, NC) using a Thermo Scientific Multidrop Combi (Thermo Fisher Scientific Inc., Waltham, MA). The media used for plating was DMEM supplemented with 10% Hyclone™ FBS and 100 U/mL penicillin and 100 μg/mL streptomycin. After the assay plates were incubated at 37 °C/5% CO_2 for 5 h, 23 nL of compounds dissolved in dimethyl sulfoxide (DMSO), CITCO (Sigma-Aldrich Corp., St. Louis, MO), or DMSO were transferred to the assay plates by a Wako Pintool station (Wako Automation, San Diego, CA). One μL of PK11195 (Sigma-Aldrich Corp.) was added (final concentration of 0.75 μM PK11195) using a Flying Reagent Dispenser (FRD, Aurora Discovery, Carlsbad, CA). The final test compound concentrations in the 5 μL assay volume ranged from 6.41 pM to 92 μM in 16 different concentrations at a 1:3 dilution. The final concentration of DMSO (used for the negative control) was 0.46%. The plate format of the positive control is as follows: Column 1: concentration-response titration of CITCO from 2.81 nM to 92 μM at a 1:2 dilution with DMSO; Column 2 top half: 60 μM of CITCO; Column 2 bottom half: 48 μM of CITCO; Column 3 top half and Column 4: DMSO only; Column 3 bottom half: 92 μM of tetraoctyl ammonium bromide. After 23 h of incubation at 37 °C/5% CO_2, one μL of CellTiter-Fluor™ (Promega, Madison, WI) was added, using the FRD, after which, all plates were put back into the incubator at 37 °C/5% CO_2 for another hour. The fluorescence intensity was then measured at 540 nm following excitation at 405 nm using a ViewLux plate reader (Perkin Elmer, Shelton, CT) to determine cell viability. Immediately after, 4 μL of ONE-Glo™ Luciferase reagent (Promega) was added to each well using the FRD and a 30 min incubation at room temperature occurred. Luminescence intensity was then measured using the ViewLux plate reader and data was expressed in relative luminescence units.

3.6. Molecular modeling and docking

The hCAR LBD was acquired as a Protein Data Bank (pdb) file and as a 2fo-fc DSN6 electron density file from the from the RCSB Protein Data Bank (http://www.rcsb.org). The PyMOL software (Schrödinger, New York, NY) was employed to remove the water molecules from the crystal structure and to display the amino acids of interest in the LBD. The ligand structures were generated as flat drawings in ChemDraw 15 (PerkinElmer, Waltham, MA), converted to 3D structures in Avogadro (Avogadro Chemistry) with energy minimization, and then converted into PDBQT files in AutoDock Tools (The Scripps Research Institute, La Jolla, CA). Docking was performed using the AutoDock Vina software (The Scripps Research Institute, La Jolla, CA). The protein search space at the XYZ dimensions was set to 15 Å × 15 Å x 15 Å. Visualization of the docking results was performed in PyMOL.

Associated content

Supporting information

The Supporting Information is available free of charge on the ACS Publications website at DOI:

General experimental procedures, supplementary data, and copies of ^1H and ^{13}C NMR spectra (PDF).

Author contributions

The manuscript was written through contributions of all authors. All authors have given approval to the final version of the manuscript.

Declaration of competing interest

The authors declare that they have no known competing financial interests or personal relationships that could have appeared to influence the work reported in this paper.

Acknowledgement

We thank the Samuel Waxman Cancer Research Foundation for their funding support to FX. We are grateful to Dr. Kellie Hom of the Department of Pharmaceutical Sciences, University of Maryland School of Pharmacy, for her technical advice on our NMR experiments. The X-ray crystallographic work was supported by NIDA through an Interagency Agreement #Y1-DA1101 with the Naval Research Laboratory (NRL).

Appendix A. Supplementary data

Supplementary data to this article can be found online at https://doi.org/10.1016/j.tet.2020.131886.

References

[1] J.M. Maglich, D.J. Parks, L.B. Moore, J.L. Collins, B. Goodwin, A.N. Billin, C.A. Stoltz, S.A. Kliewer, M.H. Lambert, T.M. Willson, J.T. Moore, Identification of a novel human constitutive androstane receptor (CAR) agonist and its use in the identification of CAR target genes, J. Biol. Chem. 278 (2003) 17277−17283.
[2] Y.E. Timsit, M. Negishi, P.X.R. Car and, The xenobiotic-sensing receptors, Steroids 72 (2007) 231−246.
[3] A. Moreau, M.J. Vilarem, P. Maurel, J.M. Pascussi, Xenoreceptors CAR and PXR activation and consequences on lipid metabolism, glucose homeostasis, and inflammatory response, Mol. Pharm. 5 (2008) 35−41.
[4] J. Gao, W. Xie, Pregnane X receptor and constitutive androstane receptor at the crossroads of drug metabolism and energy metabolism, Drug Metab. Dispos. 38 (2010) 2091−2095.
[5] H. Yang, H. Wang, Signaling control of the constitutive androstane receptor (CAR), Protein Cell 5 (2014) 113−123.
[6] W. Lin, M. Bwayi, J. Wu, Y. Li, S.C. Chai, A.D. Huber, T. Chen, CITCO directly binds to and activates human pregnane X receptor, Mol. Pharm. 97 (2020) 180−190.
[7] R. Shizu, M. Osabe, L. Perera, R. Moore, T. Sueyoshi, M. Negishi, Phosphorylated nuclear receptor CAR forms a homodimer to repress its constitutive activity for ligand activation, Mol. Cell Biol. 37 (2017) e00649-16/1-e00649-16/13.
[8] M. Pascual, M.J. Gomez-Lechon, J.V. Castell, R. Jover, ATF5 is a highly abundant liver-enriched transcription factor that cooperates with constitutive androstane receptor in the transactivation of CYP2B6: implications in hepatic stress responses, Drug Metab. Dispos. 36 (2008) 1063−1072.
[9] E.M. Laurenzana, T. Chen, M. Kannuswamy, B.E. Sell, S.C. Strom, Y. Li, C.J. Omiecinski, The orphan nuclear receptor DAX-1 functions as a potent corepressor of the constitutive androstane receptor (NR1I3), Mol. Pharm. 82 (2012) 918−928.
[11] H. de Boussac, C. Gondeau, P. Briolotti, C. Duret, F. Treindl, M. Romer, J.-M. Fabre, A. Herrero, J. Ramos, P. Maurel, M. Templin, S. Gerbal-Chaloin, M. Daujat-Chavanieu, Epidermal growth factor represses constitutive androstane receptor expression in primary human hepatocytes and favors

regulation by pregnane X receptor, Drug Metab. Dispos. 46 (2018) 223–236.
[12] T. Chen, E.M. Laurenzana, D.M. Coslo, F. Chen, C.J. Omiecinski, Proteasomal interaction as a critical activity modulator of the human constitutive androstane receptor, Biochem. J. 458 (2014) 95–107.
[13] M. Thomas, C. Bayha, S. Vetter, U. Hofmann, M. Schwarz, U.M. Zanger, A. Braeuning, Activating and inhibitory functions of WNT/β-catenin in the induction of cytochromes P450 by nuclear receptors in HepaRG cells, Mol. Pharm. 87 (2015) 1013–1020.
[14] S.S. Ferguson, Y. Chen, E.L. LeCluyse, M. Negishi, J.A. Goldstein, Human CYP2C8 is transcriptionally regulated by the nuclear receptors constitutive androstane receptor, pregnane X receptor, glucocorticoid receptor, and hepatic nuclear factor 4α, Mol. Pharm. 68 (2005) 747–757.
[15] K. Oshida, N. Vasani, C. Jones, T. Moore, S. Hester, S. Nesnow, S. Auerbach, D.R. Geter, L.M. Aleksunes, R.S. Thomas, D. Applegate, C.D. Klaassen, J.C. Corton, Identification of chemical modulators of the constitutive activated receptor (CAR) in a gene expression compendium, Nucl. Recept. Signal. 13 (2015) e002/1–e002/21.
[16] B.A. Kandel, M. Thomas, S. Winter, G. Damm, D. Seehofer, O. Burk, M. Schwab, U.M. Zanger, Genomewide comparison of the inducible transcriptomes of nuclear receptors CAR, PXR and PPARα in primary human hepatocytes, Biochim. Biophys. Acta, Gene Regul. Mech. 1859 (2016) 1218–1227.
[17] J.E. Moscovitz, A.S. Kalgutkar, K. Nulick, N. Johnson, Z. Lin, T.C. Goosen, Y. Weng, Establishing transcriptional signatures to differentiate PXR-, CAR-, and AhR-mediated regulation of drug metabolism and transport genes in cryopreserved human hepatocytes, J. Pharmacol. Exp. Therapeut. 365 (2018) 262–271.
[18] J. Lemmen, I.E.P. Tozakidis, P. Bele, H.-J. Galla, Constitutive androstane receptor upregulates Abcb1 and Abcg2 at the blood-brain barrier after CITCO activation, Brain Res. 1501 (2013) 68–80.
[19] M.A. Gray, E.J. Squires, Effects of nuclear receptor transactivation on steroid hormone synthesis and gene expression in porcine Leydig cells, J. Steroid Biochem. Mol. Biol. 133 (2013) 93–100.
[20] M. Qatanani, D.D. Moore, Car, The continuously advancing receptor, in drug metabolism and disease, Curr. Drug Metabol. 6 (2005) 329–339.
[21] L.A. Stanley, B.C. Horsburgh, J. Ross, N. Scheer, C.R. Wolf, C.A.R. Pxr and, Nuclear receptors which play a pivotal role in drug disposition and chemical toxicity, Drug Metab. Rev. 38 (2006) 515–597.
[22] W.D. Hedrich, H.E. Hassan, H. Wang, Insights into CYP2B6-mediated drug-drug interactions, Acta Pharm. Sin. B 6 (2016) 413–425.
[23] W.D. Hedrich, J. Xiao, S. Heyward, Y. Zhang, J. Zhang, M.R. Baer, H.E. Hassan, H. Wang, Activation of the constitutive androstane receptor increases the therapeutic index of CHOP in lymphoma treatment, Mol. Canc. Therapeut. 15 (2016) 392–401.
[24] V. Croixmarie, T. Umbdenstock, O. Cloarec, A. Moreau, J.-M. Pascussi, C. Boursier-Neyret, B. Walther, Integrated comparison of drug-related and drug-induced ultra performance liquid chromatography/mass spectrometry metabonomic profiles using human hepatocyte cultures, Anal. Chem. 81 (2009) 6061–6069.
[25] H. Li, T. Chen, J. Cottrell, H. Wang, Nuclear translocation of adenoviral-enhanced yellow fluorescent protein-tagged-human constitutive androstane receptor (hCAR): a novel tool for screening hCAR activators in human primary hepatocytes, Drug Metab. Dispos. 37 (2009) 1098–1106.
[26] C. Lynch, Y. Pan, L. Li, S.S. Ferguson, M. Xia, P.W. Swaan, H. Wang, Identification of novel activators of constitutive androstane receptor from FDA-approved drugs by integrated computational and biological approaches, Pharm. Res. 30 (2013) 489–501.
[27] A. Carazo, P. Pavek, The use of the LanthaScreen TR-FRET CAR coactivator assay in the characterization of constitutive androstane receptor (CAR) inverse agonists, Sensors 15 (2015) 9265–9276.
[28] V. Soldatow, R.C. Peffer, O.J. Trask, D.E. Cowie, M.E. Andersen, E. LeCluyse, C. Deisenroth, Development of an in vitro high content imaging assay for quantitative assessment of CAR-dependent mouse, rat, and human primary hepatocyte proliferation, Toxicol. In Vitro 36 (2016) 224–237.
[29] K. Kobayashi, Y. Yamanaka, N. Iwazaki, I. Nakajo, M. Hosokawa, M. Negishi, K. Chiba, Identification of HMG-CoA reductase inhibitors as activators for human, mouse and rat constitutive androstane receptor, Drug Metab. Dispos. 33 (2005) 924–929.
[30] J. Kueblbeck, T. Laitinen, J. Jyrkkaerinne, T. Rousu, A. Tolonen, T. Abel, T. Kortelainen, J. Uusitalo, T. Korjamo, P. Honkakoski, F. Molnar, Use of comprehensive screening methods to detect selective human CAR activators, Biochem. Pharmacol. 82 (2011) 1994–2007.
[31] A.J. Lau, G. Yang, T.K.H. Chang, Isoform-selective activation of human constitutive androstane receptor by Ginkgo biloba extract: functional analysis of the SV23, SV24, and SV25 splice variants, J. Pharmacol. Exp. Therapeut. 339 (2011) 704–715.
[32] F. Al-Salman, N. Plant, Non-coplanar polychlorinated biphenyls (PCBs) are direct agonists for the human pregnane-X receptor and constitutive androstane receptor, and activate target gene expression in a tissue-specific manner, Toxicol. Appl. Pharmacol. 263 (2012) 7–13.
[33] T. Sueyoshi, L. Li, H. Wang, R. Moore, P.R.S. Kodavanti, H.-J. Lehmler, M. Negishi, L.S. Birnbaum, Flame retardant BDE-47 effectively activates nuclear receptor CAR in human primary hepatocytes, Toxicol. Sci. 137 (2014) 292–302.
[34] E.A. Rondini, Z. Duniec-Dmuchowski, T.A. Kocarek, Nonsterol isoprenoids activate human constitutive androstane receptor in an isoform-selective manner in primary cultured mouse hepatocytes, Drug Metab. Dispos. 44 (2016) 595–604.
[35] T. Smutny, A. Nova, M. Drechslerova, A. Carazo, L. Hyrsova, Z.R. Hruskova, J. Kunes, M. Pour, M. Spulak, P. Pavek, 2-(3-Methoxyphenyl)quinazoline derivatives: a new class of direct constitutive androstane receptor (CAR) agonists, J. Med. Chem. 59 (2016) 4601–4610.
[36] Y. Kanno, N. Tanuma, T. Yatsu, W. Li, K. Koike, Y. Inouye, Nigramide J is a novel potent inverse agonist of the human constitutive androstane receptor, Pharmacol Res Perspect 2 (2014) 2.
[37] H.-Y. Chang, C.-J. Chen, W.-C. Ma, W.-K. Cheng, Y.-N. Lin, Y.-R. Lee, J.-J. Chen, Y.-P. Lim, Modulation of pregnane X receptor (PXR) and constitutive androstane receptor (CAR) activation by ursolic acid (UA) attenuates rifampin-isoniazid cytotoxicity, Phytomedicine 36 (2017) 37–49.
[38] J. Kublbeck, J. Jyrkkarinne, F. Molnar, T. Kuningas, J. Patel, B. Windshugel, T. Nevalainen, T. Laitinen, W. Sippl, A. Poso, P. Honkakoski, New in vitro tools to study human constitutive androstane receptor (CAR) biology: discovery and comparison of human CAR inverse agonists, Mol. Pharm. 8 (2011) 2424–2433.
[39] D. Liang, L. Li, C. Lynch, B. Diethelm-Varela, M. Xia, F. Xue, H. Wang, DL5050, a selective agonist for the human constitutive androstane receptor, ACS Med. Chem. Lett. 10 (2019) 1039–1044.
[40] D. Liang, L. Li, C. Lynch, B. Mackowiak, W.D. Hedrich, Y. Ai, Y. Yin, S. Heyward, M. Xia, H. Wang, F. Xue, Human constitutive androstane receptor agonist DL5016: a novel sensitizer for cyclophosphamide-based chemotherapies, Eur. J. Med. Chem. 179 (2019) 84–99.
[41] R.X. Xu, M.H. Lambert, B.B. Wisely, E.N. Warren, E.E. Weinert, G.M. Waitt, J.D. Williams, J.L. Collins, L.B. Moore, T.M. Willson, J.T. Moore, A structural basis for constitutive activity in the human CAR/RXRα heterodimer, Mol. Cell *16* (2004) 919–928.
[42] M.E. Muratore, C.A. Holloway, A.W. Pilling, R.I. Storer, G. Trevitt, D.J. Dixon, Enantioselective Bronsted acid-catalyzed N-acyliminium cyclization cascades, J. Am. Chem. Soc. 131 (2009) 10796–10797.
[43] R.M. Parrish, L.A. Burns, D.G.A. Smith, A.C. Simmonett, A.E. DePrince 3rd, E.G. Hohenstein, U. Bozkaya, A.Y. Sokolov, R. Di Remigio, R.M. Richard, J.F. Gonthier, A.M. James, H.R. McAlexander, A. Kumar, M. Saitow, X. Wang, B.P. Pritchard, P. Verma, H.F. Schaefer 3rd, K. Patkowski, R.A. King, E.F. Valeev, F.A. Evangelista, J.M. Turney, T.D. Crawford, C.D. Sherrill, Psi4 1.1: an open-source electronic structure program emphasizing automation, advanced libraries, and interoperability, J. Chem. Theor. Comput. 13 (2017) 3185–3197.
[44] J.E. Johnson, N.M. Morales, A.M. Gorczyca, D.D. Dolliver, M.A. McAllister, Mechanisms of acid-catalyzed Z/E isomerization of imines, J. Org. Chem. 66 (2001), 7979-7685.
[45] J.S. Wu, W.M. Liu, X.Q. Zhuang, F. Wang, P.F. Wang, S.L. Tao, X.H. Zhang, S.K. Wu, S.T. Lee, Fluorescence turn on of coumarin derivatives by metal cations: a new signaling mechanism based on C=N isomerization, Org. Lett. 9 (2007) 33–36.
[46] W.F. Schmid, R.O. John, G. Muhlgassner, P. Heffeter, M.A. Jakupec, M. Galanski, W. Berger, V.B. Arion, B.K. Keppler, Metal-based paullones as putative CDK inhibitors for antitumor chemotherapy, J. Med. Chem. 50 (2007), 6343-5355.
[47] E.A. Rodkey, D.C. McLeod, C.R. Bethel, K.M. Smith, Y. Xu, W. Chai, T. Che, P.R. Carey, R.A. Bonomo, F. van den Akker, J.D. Buynak, beta-Lactamase inhibition by 7-alkylidenecephalosporin sulfones: allylic transposition and formation of an unprecedented stabilized acyl-enzyme, J. Am. Chem. Soc. 135 (2013) 18358–18369.
[48] C. Lynch, J. Zhao, R. Huang, J. Xiao, L. Li, S. Heyward, M. Xia, H. Wang, Quantitative high-throughput identification of drugs as modulators of human constitutive androstane receptor, Sci. Rep. 5 (2015) 10405.
[49] S. Emami, A. Foroumadi, One-pot sequential synthesis of O-(halo-substituted benzyl) hydroxylammonium salts, Arab. J. Chem. 10 (2017) S225–S229.